



Failure prediction by using a recurrent neural network in incremental sheet forming with active medium

Thiery, Sebastian; Zein El Abdine, Mazhar; Heger, Jens; Ben Khalifa, Noomane

Published in:

International Journal of Material Forming

DOI:

[10.1007/s12289-025-01957-w](https://doi.org/10.1007/s12289-025-01957-w)

Publication date:

2025

Document Version

Publisher's PDF, also known as Version of record

[Link to publication](#)

Citation for published version (APA):

Thiery, S., Zein El Abdine, M., Heger, J., & Ben Khalifa, N. (2025). Failure prediction by using a recurrent neural network in incremental sheet forming with active medium. *International Journal of Material Forming*, 18(4), Article 91. <https://doi.org/10.1007/s12289-025-01957-w>

General rights

Copyright and moral rights for the publications made accessible in the public portal are retained by the authors and/or other copyright owners and it is a condition of accessing publications that users recognise and abide by the legal requirements associated with these rights.

- Users may download and print one copy of any publication from the public portal for the purpose of private study or research.
- You may not further distribute the material or use it for any profit-making activity or commercial gain
- You may freely distribute the URL identifying the publication in the public portal ?

Take down policy

If you believe that this document breaches copyright please contact us providing details, and we will remove access to the work immediately and investigate your claim.



Failure prediction by using a recurrent neural network in incremental sheet forming with active medium

Sebastian Thiery¹ · Mazhar Zein El Abdine¹ · Jens Heger¹ · Noomane Ben Khalifa^{1,2}

Received: 11 December 2024 / Accepted: 15 October 2025
© The Author(s) 2025

Abstract

Industrial sheet metal components often have complex geometries with both concave and convex features. For small batch sizes, such components can be manufactured by incremental sheet forming, using the pressure of an active medium underneath the workpiece to create the convex feature. However, the additional load superimposed by the pressure causes instability and renders the process more prone to failure, in particular to cracking of the workpiece. The reliability of the manufacturing process could be improved if the occurrence of failure were predictable and thus preventable. To achieve this goal, the trend of the forming forces and the change of the workpiece geometry prior to cracking are experimentally analyzed. Subsequently, the dataset obtained from the experiments is used to fit a model based on long short-term memory and on a sliding window approach. This model reliably predicts the probability of failure with an accuracy and recall of 0.97 and 0.89 respectively, demonstrating its potential for online monitoring of the manufacturing process.

Keywords Incremental sheet forming · Active medium · Failure prediction · Long short-term memory · Process monitoring

Introduction

High flexibility and low costs are decisive advantages of incremental sheet forming (ISF) processes to manufacture customized products for medical purposes or prototypes for industrial applications. Sheet metal components can have different degrees of complexity ranging from axisymmetric truncated cones to irregular shapes with both concave and convex features. Several strategies have been developed

regarding the support of the workpiece and monitoring of the manufacturing process to ensure a reliable production procedure and to optimize the part quality. Since monitoring approaches rely on data obtained from sensors within the setup, solutions based on artificial intelligence (AI) provide new opportunities to enhance the industrial applicability of ISF.

The common feature of ISF processes is the fact that a small punch follows the contours of the target shape in three-dimensional space and forms the workpiece step by step. Concave components can be manufactured by an ISF type known as single point incremental forming (SPIF), in which the sheet metal is clamped at the circumference but has no solid support [1]. SPIF has higher forming limits than conventional sheet metal forming processes such as deep drawing [2]. However, sheet thinning is subjected to the sine law, which leads to fracture when the maximum wall angle is reached [3]. Skjoedt et al. [4] investigated the limits of AA1050-O aluminum sheets and reported a maximum wall angle of 77.5°, corresponding to a thickness reduction from 1.00 mm to 0.22 mm. Even though the forming limits of SPIF could be extended by multi-stage strategies, process limitations regarding geometrical complexity and accuracy remain [5]. The range of achievable geometries can be

✉ Sebastian Thiery
sebastian.thiery@leuphana.de

Mazhar Zein El Abdine
mazhar.abdine@leuphana.de

Jens Heger
jens.heger@leuphana.de

Noomane Ben Khalifa
noomane.ben_khalifa@leuphana.de

¹ Institute for Production Technology and Systems, Leuphana University Lüneburg, Universitätsallee 1, 21335 Lüneburg, Germany

² Institute of Material and Process Design, Helmholtz-Zentrum Hereon, Max-Planck-Str. 1, 21502 Geesthacht, Germany

expanded using a solid die (two point incremental forming, TPIF) or a second movable tool (double sided incremental forming, DSIF). Moreover, such additional equipment can be used to exert counterpressure on the workpiece and thus influence the forming process through stress superposition. For example, TPIF can be combined with stretch forming to induce tensile stresses [6], or a predefined force can be applied by the second tool in DSIF [7].

By including a pressurized medium to support the sheet, referred to as incremental sheet forming with active medium (IFAM), convex shapes can be created by controlled upwards bulging of the material [8]. The geometry of the workpiece is the result of the interaction between the pressure of the medium and the force provided by the tool movement. In addition, concave forming operations by SPIF can be performed to produce a component with combined geometrical features. With this strategy, complex components can be manufactured without the need for a solid die or a second movable tool. However, the pressure of the medium superimposes a static load into the material, causing instability for high wall angles and increases the probability for cracks [8]. Thiery et al. [9] reported cracks for conditions with both high pressure and large strains and showed that the maximum achievable part height is limited when using a constant pressure throughout the manufacturing process. In general, ISF is characterized by local deformation of the material [10]. Ben Khalifa and Thiery [8] showed by means of a numerical investigation that the material deformation in IFAM occurs in the contact region between tool and workpiece and thus corresponds to the mechanics of ISF.

Monitoring strategies to detect or to predict sheet failure improve the efficiency of the manufacturing process by saving costs and time. These strategies are based on sensory data obtained directly from the process operation where notably the forming forces can be easily accessed. The forces in three spatial dimensions F_z , F_x and F_y can be measured by integrating a table type force sensor between the fixture holding the blank and the bench of the milling machine [11]. To that end, Aereus et al. [12] propose a procedure to calculate the tangential force F_t in direction of the tool movement and the radial force F_r orientated perpendicular to the tool movement while manufacturing a truncated cone. Different frameworks exist to correlate the occurrence of failure with the trend of one of these force components. The work of Petek et al. [13] focuses on the vertical force to detect the onset of cracks for the case of an irregular shape with several corners. The force trend exhibits peaks when the tool moves along the corners since the contact area between tool and workpiece increases and biaxial stretching of the material prevails in these positions. The cracks most likely occur in the corners and the corresponding force peaks disappear in this case. By the change in the force trend, the crack can

then be autonomously identified [13]. On the other hand, the tangential force shows a monotonically decreasing trend with a negative gradient for high wall angles eventually resulting into cracks [14]. Sound parts with moderate wall angle demonstrate a peak followed by a steady-state behavior in the trend of the tangential force. Therefore, the behavior of the tangential force can be used as indicator for imminent cracks so that the tool radius and the step size can be adapted in order to avoid the failure [15]. Moreover, Fiorentino [16] proposed a framework to calculate a reference stress based on the vertical and the tangential forming force in combination with process parameters and material constants. In this way, a force-based criterion can be defined to identify critical stress states before a crack occurs in convex TPIF [16].

The increasing deployment of sensors into manufacturing processes and developments such as the Industrial Internet of Things, both essential aspects of the digital transformation in the industry, provide the opportunity to collect a large amount of data [17]. Hence, AI-based techniques can be applied to design or control a manufacturing process, ensuring the quality meets the demands. Cao et al. [18] focus in their review on potential applications of AI in metal forming processes and identify possible directions for future research. In particular, AI-based methods can be used to solve problems that are related to ISF [19]. Ambrogio and Filice [20] developed an approach to predict material failure in SPIF based on artificial neural networks (ANN), performing experiments with varying wall angles while other process parameters were kept constant. With the wall angle as input, this model can predict the part height on which failure occurs and can therefore be used to check the feasibility of a geometry in advance [21]. Nevertheless, the experiments in SPIF are time-consuming and restrict the possibility to create rich datasets. On the one hand, Liu and Li [22] proposed a strategy to generate virtual data based on mega trend diffusion function and particle swarm optimization algorithm. This strategy reduces the amount of data required to train a model as was demonstrated on 34 experiments for predicting the forming force in dependency of the step size, the sheet thickness, the tool diameter and the wall angle in SPIF [22]. On the other hand, Duan et al. [23] investigated a transfer learning approach based on graph neural networks for predicting the forming force in DSIF. In this strategy, the model is pretrained on a dataset generated by manufacturing of different geometries. For the case of varying material properties, the pretrained model cannot accurately predict the forming force without additional measures. Therefore, the model was calibrated during the first contours of the tool-path and was afterwards used to predict the forming force for the rest of the contours, proving that it is not necessary to repeat all experiments of the training phase [23]. Regarding

IFAM, Thiery et al. [9] performed experiments on convex truncated cones to identify the correlation between the pressure of the active medium and the increase of part height during one contour of the toolpath. After extrapolation of the data, an ANN-based model was trained and used as controller to predict the pressure for each contour in a discrete closed-loop control concept [9].

Depending on the application and the format of the data, different types of ANNs such as feed-forward neural networks, convolutional neural networks and recurrent neural networks (RNN) can be chosen [24]. In the recent years, algorithms for time-series pattern recognition experienced increasing interest [25]. RNNs and especially algorithms with long short-term memory (LSTM) are designed in such way that they have a time-awareness and can save information from previous data points, making them a favorable tool for time series-analytics [25]. In machining, where the cutting parameters and other measurement values are continuously recorded during the manufacturing processes, the potential of time-aware algorithms becomes clear. Manjunath et al. [26] showed that LSTM modelling is capable of predicting the surface roughness after milling operations in dependency of the cutting parameters. Ma et al. [27] conducted 195 cutting experiments and measured both the cutting force during the experiments and the tool wear after the experiments. They developed an approach based on CNN and LSTM to estimate the tool wear using the force as input [27]. A similar architecture was applied by Peng et al. [28] to predict the milling force based on the spindle current signal. Though time series-analytics was successfully employed for different cases considering milling machines and the transfer of these methods to ISF would be possible, there is no research in this regard existing in the literature. However, the identification of failures in metal forming using time-aware models is generally possible as proven by investigations on cold rolling [29] and deep drawing [30].

From the literature can be concluded that AI-based modelling approaches with memory function have an advantage over conventional methods of machine learning for processing time-series data. Nevertheless, the potential of these models for application in ISF has not yet been investigated. In particular, the prediction of failure in IFAM would be a suitable application for time-aware models and would increase the reliability of the manufacturing process because cracks could be avoided prior to their occurrence. To pursue this goal, experiments with varying step size and pressure levels are conducted to capture the forming behavior until failure. A dataset including the average value of the forming force component, part height and geometry of the toolpath for each contour is extracted from the experiments. Subsequently, an LSTM-model is trained and evaluated for predicting failures.

Methodology

Convex forming by active medium

The definition of incremental sheet forming includes the characteristic that the tool moves in three-dimensional space following a predefined target geometry [31]. In this regard, the information about the target geometry is stored within the toolpath as is common for kinematic forming processes. In two point incremental forming, the workpiece can be supported by a dedicated die to create convex shapes, Fig. 1a. In this case, the workpiece is fixed to a movable plate above the die. The tool starts with the top contour and moves downwards with every subsequent contour until the process is finished. During the process, the top of the workpiece is supported by the die while the margin is pushed towards the bottom by the tool.

Another strategy to shape convex components is to replace the solid die by an active medium [8]. A closed space is created by attaching the workpiece onto the top of the pressure chamber, and subsequently the pressure of the active medium is applied, Fig. 1b. The tool starts with the inner contour and moves outwards with each contour until the process is finished. A small part of the final component emerges with every contour of the toolpath. In this case, the margin of the workpiece is fixed by the blankholder and the top moves upwards due to the pressure. The pressure of the active medium is set low so that plastic yielding only occurs in the contact region between tool and workpiece. Neither the tool nor the active medium would lead to plastic yielding if not combined.

A particularity of incremental sheet forming with active medium is the fact that the toolpath is two-dimensional. Once the tool is positioned on the upper surface of the workpiece, it moves predominantly in the horizontal plane. However, the reduction of the three-dimensional target geometry to a two-dimensional toolpath represents a loss of geometrical information. The toolpath describes the outline of the component without specifying the vertical position. Nonetheless, the wall angle as well as the degree of plastic deformation can be influenced by the pressure of the active medium. A high pressure level increases the resulting wall angle whereas a low pressure level will create a shallow component. By adjusting the pressure, missing geometrical information can be compensated for. Moreover, conditions with high pressure and high wall angle have a risk for the occurrence of cracks.

Experimental set-up

A chamber is used to apply the pressure of an active medium, in this case pressurized air, on the bottom surface of the

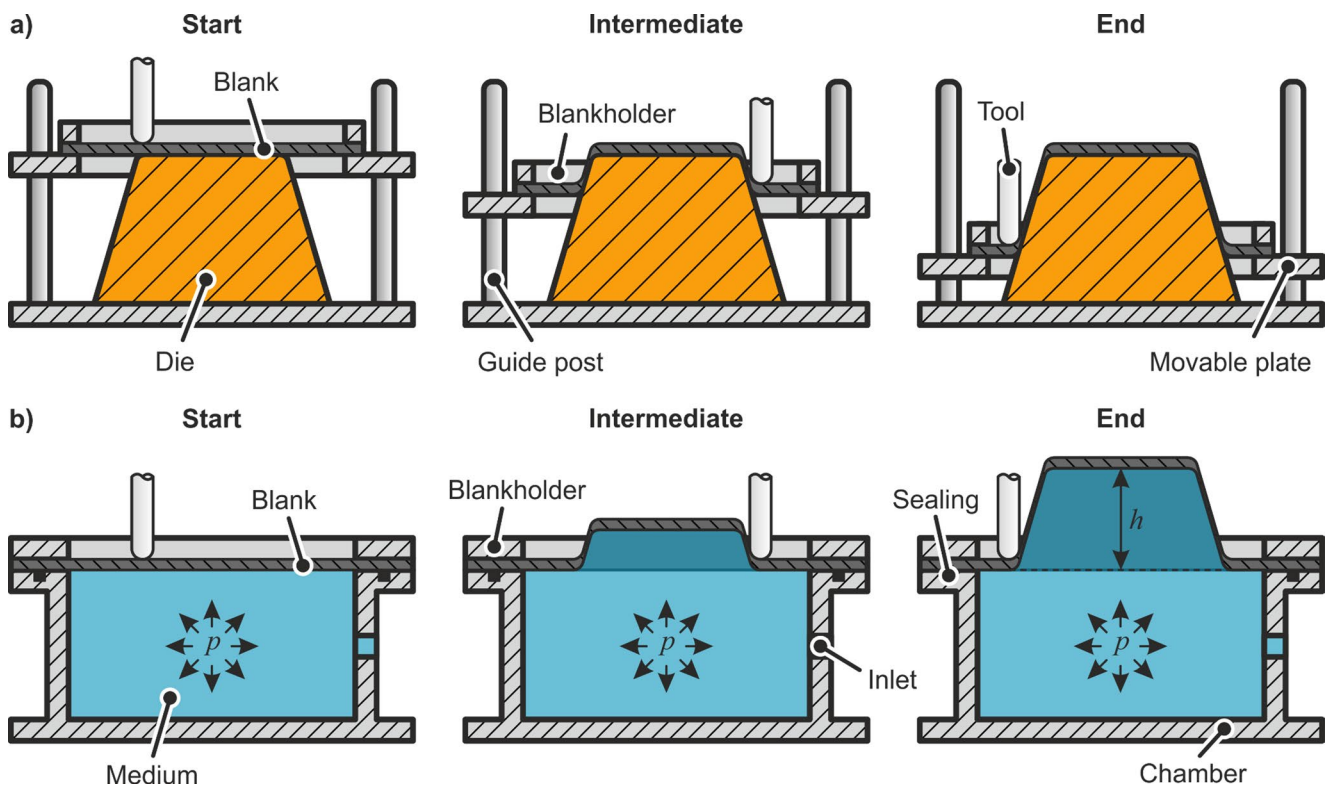


Fig. 1 Forming convex truncated cones (a) by two point incremental forming and (b) using an active medium

workpiece, Fig. 2. The pressure required to create convex shapes by upwards bulging of the material is, in comparison to conventional hydroforming processes, significantly lower. Ben Khalifa and Thiery [8] showed that a pressure of $p = 0.35$ bar relative to atmospheric pressure can lead to cracks for certain toolpaths. Moreover, there is space with depth of 100 mm inside the chamber so that it is possible to perform concave forming operation via SPIF with the same set-up. When the workpiece is fixed by clamping on the top of the pressure chamber, a rubber sealing underneath the workpiece avoids leakages. The dimensions within the clamping are 190 mm x 190 mm, whereas the total dimensions of the workpiece clamped are 280 mm x 280 mm. The experiments are performed with pure aluminum AA1050A-H24 with a thickness of $s = 1$ mm. The top surface of the workpiece is lubricated with forming oil to reduce the friction with the tool. The tool has a hemispherical tip with a radius of $R = 5$ mm.

A computer is placed in the vicinity of the milling machine to record the sensor signals by a measurement and control software written in LABVIEW, Fig. 2. The software collects the analog signals from the pressure sensor, the laser distance sensors and the values from force measuring platform from AMTI type MC12-4k. In addition, it sets the target value for the pressure valve. A connection to the CNC control system is established by a local area network.

Experimental design

The toolpath in ISF is three-dimensional for most process types since the tool moves along the target geometry. However, the toolpath in IFAM is two-dimensional and the three-dimensional geometry of the product is the result of the interaction between the tool movement in the horizontal plane and the pressure of the active medium. In line with this, a spiral toolpath was designed to create convex truncated cones used for investigating the occurrence of failure, Fig. 3a. The purpose of this strategy is to avoid a sharp transition between two contours because the transition region would be a weak spot where cracks most likely would occur. In contrast, the onset of cracks is distributed over the whole contour using the spiral toolpath, Fig. 3b. Toolpaths with varying horizontal step size Δy were tested. However, the radius of the first half of the first contour is 45 mm and the radius of the second half of the last contour is minimum 75 mm for all toolpaths. The part height and the wall angle of the truncated cones are not defined beforehand but are detected throughout the manufacturing process to identify the forming limits. The vertical position of the tool is set to $z = 0$ mm throughout the whole process so that there is no gap between the top surface of the workpiece and the tip of the tool. The feed rate and rotational speed are set as by $f = 1000$ mm/min and $n = 60$ rpm, respectively.

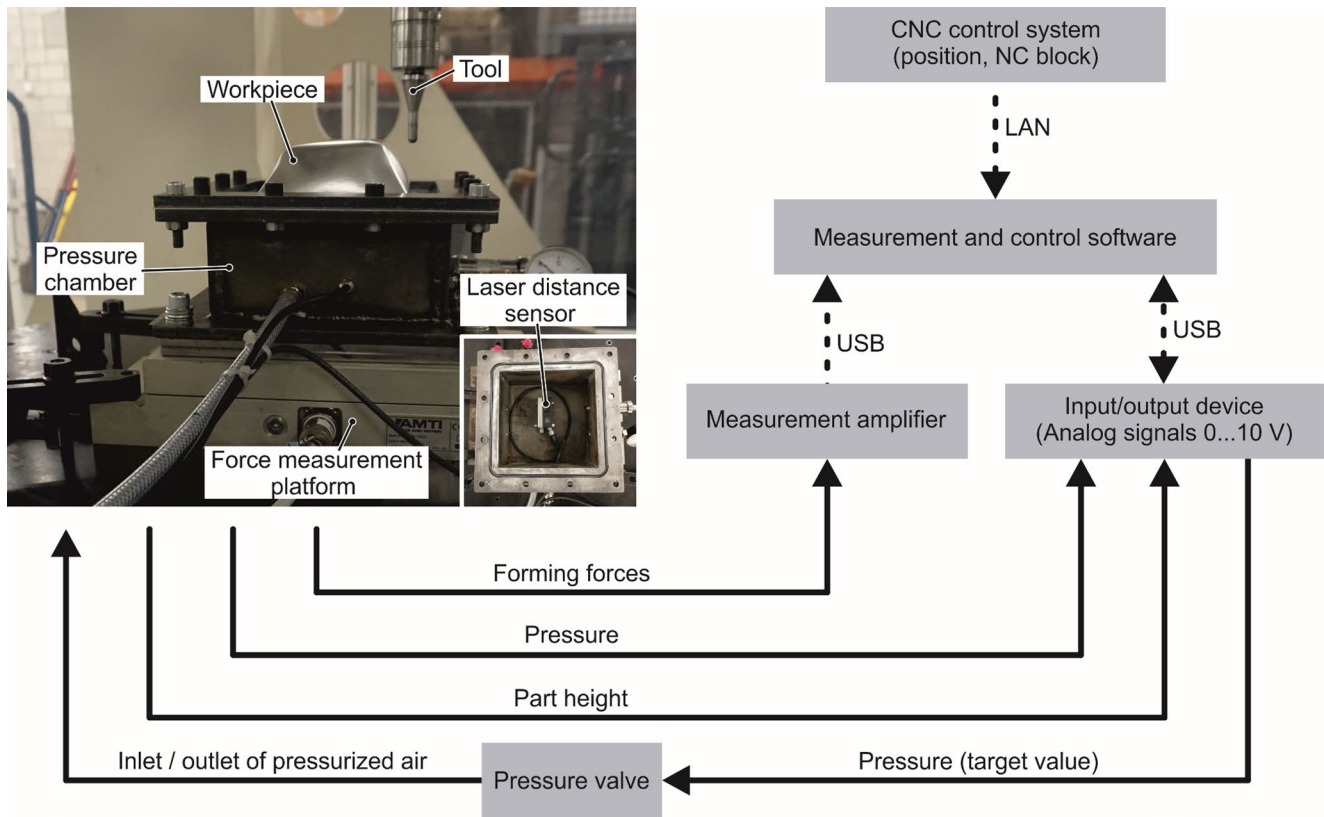


Fig. 2 Set-up of incremental sheet forming with active medium showing a truncated pyramid and interfaces for data acquisition

Fig. 3 (a) Spiral toolpath for a smooth tool movement and (b) occurrence of cracks in the manufacturing process

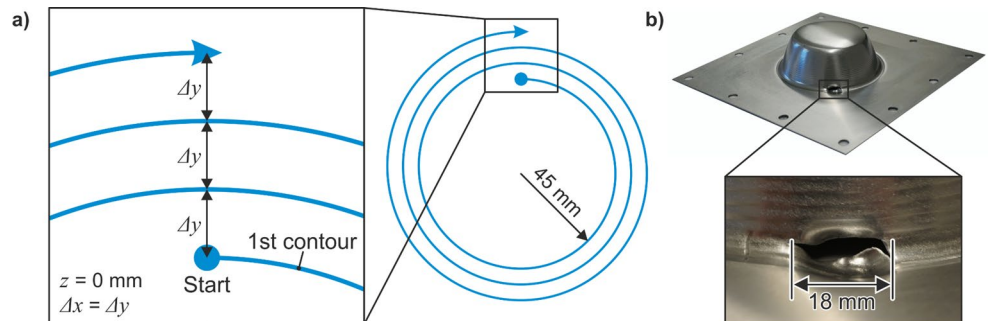


Table 1 Experimental plan to observe the occurrence of cracks at varying process progresses

Step size [mm]	Pressure [bar]
0.7	0.48–0.51–0.54–0.56–0.58
0.8	0.51–0.53–0.55–0.57–0.60
0.9	0.52–0.54–0.57–0.60–0.62
1.0	0.54–0.57–0.59–0.62–0.64
1.1	0.57–0.58–0.59–0.62–0.64

Previous studies showed that the forming process in IFAM is affected by the step size with a smaller step size increasing the sensitivity towards the pressure [8]. Hence, the experiments are performed for five values of the step size according to Table 1. For each step size, the pressure

is varied in five levels so that cracks occur earlier in the process using high pressure and later using low pressure. In total, 25 experiments are conducted until a crack appears since the pressure cannot be kept up after this event and the process needs to be stopped. The pressure is kept constant throughout the process. The spatial force components and the tool position are continuously recorded so that the tangential and the radial forming force can be determined according to Thiery et al. [32]. The NC blocks are used to synchronize the CNC control system and the measurements and control software. After a contour is completed, the mean value of the forming forces is calculated and the height of the workpiece is detected. These values are not calculated in case of a crack since the last contour is not completed until the end.

The height of the component is measured by the laser distance sensor. To describe the increase of the height during a single contour of the toolpath, the difference Δh_n between the actual height h_n and the height before the contour h_{n-1} is calculated (Eq. 1).

$$\Delta h_n = h_n - h_{n-1} \quad (1)$$

In analogy to SPIF where the ratio of horizontal step size and vertical step size relates with the wall angle [31], the wall angle of the component α_{apx} can be calculated by Eq. (2).

$$\tan \alpha_{\text{apx}} = \frac{\Delta h}{\Delta y} \quad (2)$$

The sine law for incremental sheet forming can be described by cosine to estimate sheet thinning [33]. Based on this theory, the sheet thickness s_{apx} in IFAM can be approximated by Eq. (3).

$$\cos \alpha_{\text{apx}} = \frac{s_{\text{apx}}}{s} \quad (3)$$

Sequential modelling and data Preparation

While both classical artificial neural networks (ANNs) and recurrent neural networks (RNNs) are deep learning models well-suited for handling non-linear data, they differ in their structure and functionality. In ANNs, neurons only communicate with neurons in the subsequent layers, resulting in a strictly feedforward architecture. In contrast, RNNs enable neurons to communicate not only with neurons in subsequent layers but also with neurons in preceding layers [34]. RNNs are essentially an extension of classical neural networks specifically designed to handle sequential data. They function as dynamic systems that can maintain a memory of past inputs, which influences future outputs. Hence, the same input can produce different outputs, depending on the sequence of previous inputs. This behavior is achieved by continuously feeding the output of the network back into the process, allowing it to update its internal state dynamically.

Long Short-Term Memory (LSTM) [35] and Gated Recurrent Units (GRU) [36, 37] are among the most prominent types of RNNs, particularly effective for sequential forecasting tasks. LSTM networks were designed to overcome the challenges of exploding and vanishing gradients, which often arise when propagating through many stages of a network [35]. They excel at capturing long-term dependencies by integrating multi-layered repeating modules into their architecture. Each module consists of memory cells and gates that regulate the flow of information, determining

what information to retain, discard, or update within the memory cells. Cells receive an input vector x_t and the previous hidden state h_{t-1} : the process starts with the forget gate f_t , determining which information from the previous cell state C_{t-1} to retain (Eq. 4). Next, the input gate i_t determines which new information to include in the memory cell C_t through generating candidate updates g_t (Eqs. 5, 6). The cell state is then updated by combining the retained and new information through element-wise multiplication operations (Eq. 7). Finally, the output gate o_t determines which portion of the updated cell state contributes to the hidden state h_t (Eq. 8). The latter constitutes the output of the LSTM cell and is passed to the following sequences or layers. After the input sequence has been computed within the cell, the final hidden state h_t passes through a fully connected layer with weight matrix W , bias vector b and a sigmoid activation function σ to produce a probability of crack occurrence for the following contour (Eq. 10).

During training, the model minimizes the binary cross-entropy loss (Eq. 11), where y_i is the true label and \hat{y}_i is the predicted probability of crack occurrence. The gradients are computed and optimized using backpropagation through time [34] for all weights W_f, W_i, W_c, W_o and biases b_f, b_i, b_c, b_o with learning rate η (Table 2).

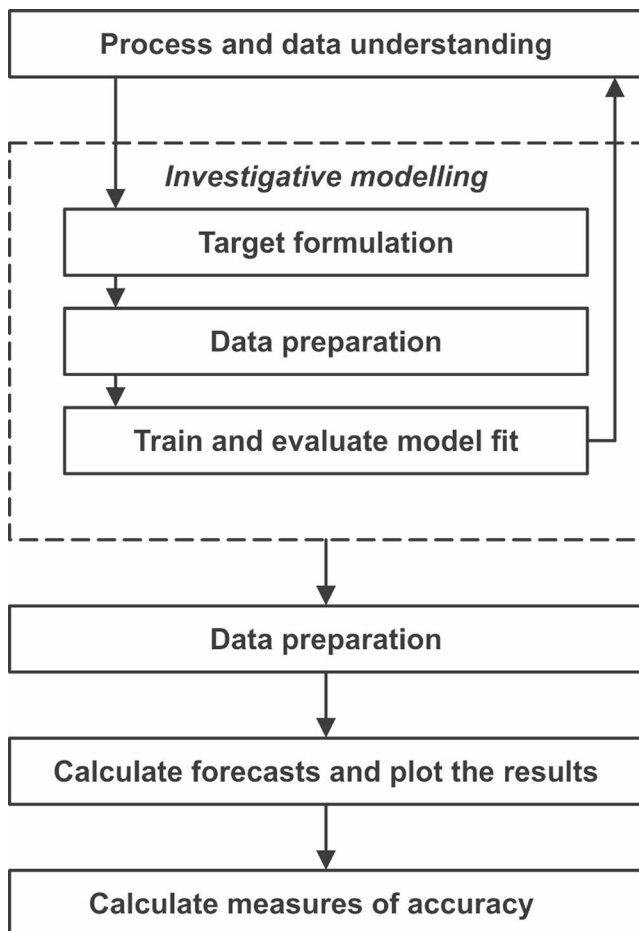
In this study, we applied a sliding window approach with data overlap to predict future values on a short-term basis. The fixed-length input sequence, here referred to as the window length, was set to three contours. This value was selected after comparing it to window lengths of five and seven contours. In other words, the model was trained to identify patterns in the data from three consecutive contours $[n-2, n-1, n]$ to forecast the occurrence of a crack in the following contour $n+1$. Afterwards, the window shifts forward by one contour, so that the next input sequence becomes $[n-1, n, n+1]$ to forecast the crack occurrence in $n+2$, and so on. All input data were min-max scaled and mapped to a range between -1 and 1 . The scaler was fitted to the training data only, preserving the integrity of the test-sets. The input data includes the part height, the three force components, the contour number n and the diameter of the contour.

Modelling approach

To model the data within the scope of a machine learning application, we referred to the CRISP-ML(Q) framework [38], which expands on the CRISP-DM [39] framework commonly used for data mining projects. CRISP-ML(Q) is specifically tailored for machine learning tasks in technical domains, Fig. 4. The framework begins with an understanding of the specific application and the data associated with it. An exploratory data analysis phase follows, where the data is inspected, cleaned, and scaled. Afterwards, an

Table 2 Step by step description of operations for training a typical LSTM model

Operation	Formulation	Reference
Input	$x_t = [x_{t,1}, x_{t,2}, x_{t,3}, x_{t,4}, x_{t,5}, x_{t,6}]$	
Forget gate	$f_t = \sigma(W_{x_f}x_t + W_{h_f}h_{t-1} + b_f)$	(4)
Input gate	$i_t = \sigma(W_{x_i}x_t + W_{h_i}h_{t-1} + b_i)$,	(5)
	$g_t = \tanh(W_{x_c}x_t + W_{h_c}h_{t-1} + b_c)$	(6)
Cell state update	$C_t = f_t \odot C_{t-1} + i_t \odot g_t$	(7)
Output gate	$o_t = \sigma(W_{x_o}x_t + W_{h_o}h_{t-1} + b_o)$,	(8)
	$h_t = o_t \odot \tanh(C_t)$	(9)
Final prediction	$\hat{y} = \sigma(W \cdot h_t + b)$	(10)
Loss computation	$L = -\frac{1}{N} \sum_{i=1}^N [y_i \log(\hat{y}_i) + (1 - y_i) \log(1 - \hat{y}_i)]$	(11)
Backpropagation	$W \leftarrow W - \eta \nabla_W L$	(12)

**Fig. 4** Framework used to develop the recurrent neural network for prediction of failure

investigative modeling phase is initiated, where various models, parameters, and hyperparameter combinations are systematically tested and evaluated. This iterative process leverages domain expertise to help assess the results for correctness and feasibility in the context of the defined targets. This phase addresses key questions related to data,

model structure, and parameter settings. Finally, in the modeling phase, the selected model architecture is fit with the refined parameters and hyperparameters and is subsequently evaluated. Most notably in this study, investigations were conducted to determine the optimal window length for the model, select the number of layers, analyze the sensitivity to hyperparameter variations, and finally to examine the influence of different data splits on the obtained results.

For the investigations, a standard 80/20 train-test split was applied, where the chronological order of the contours within the experiments was preserved. That is, the split occurs on the experiment level by assigning entire experiments to either the training or the test set. As such, the models were evaluated on entirely unseen experiments. Afterwards, the final training and evaluation were performed with a k -fold cross-validation using $k = 8$, so that from the randomly shuffled experiments, eight groups are formed, each containing three experiments. The process is repeated ten times for different random shuffles i.e. splits, resulting in a total of eighty train-validation runs. For each test group, the accuracy of the corresponding model depends on whether the occurrence of failure is predicted correctly (TP – true positive) or misclassified (FN – false negative). On the other hand, uncritical contours might be identified accurately (TN – true negative) or failure might be forecasted some contours too early (FP – false positive). By nature of the manufacturing process and the experiments conducted, the resulting dataset was highly imbalanced, containing significantly more negative cases (no crack) than positive ones (crack occurrence). Subsequently, the performance metrics Precision P (Eq. 13), Recall R (Eq. 14) and F1 score F (Eq. 15) were used next to the Accuracy A (Eq. 16) to evaluate model performance as shown in [40], as to account for the imbalance.

$$P = \frac{TP}{TP + FP} \quad (13)$$

$$R = \frac{TP}{TP + FN} \tag{14}$$

$$F = \frac{2 \cdot TP}{2 \cdot TP + FP + FN} \tag{15}$$

$$A = \frac{TP + TN}{TP + TN + FP + FN} \tag{16}$$

Results and discussion

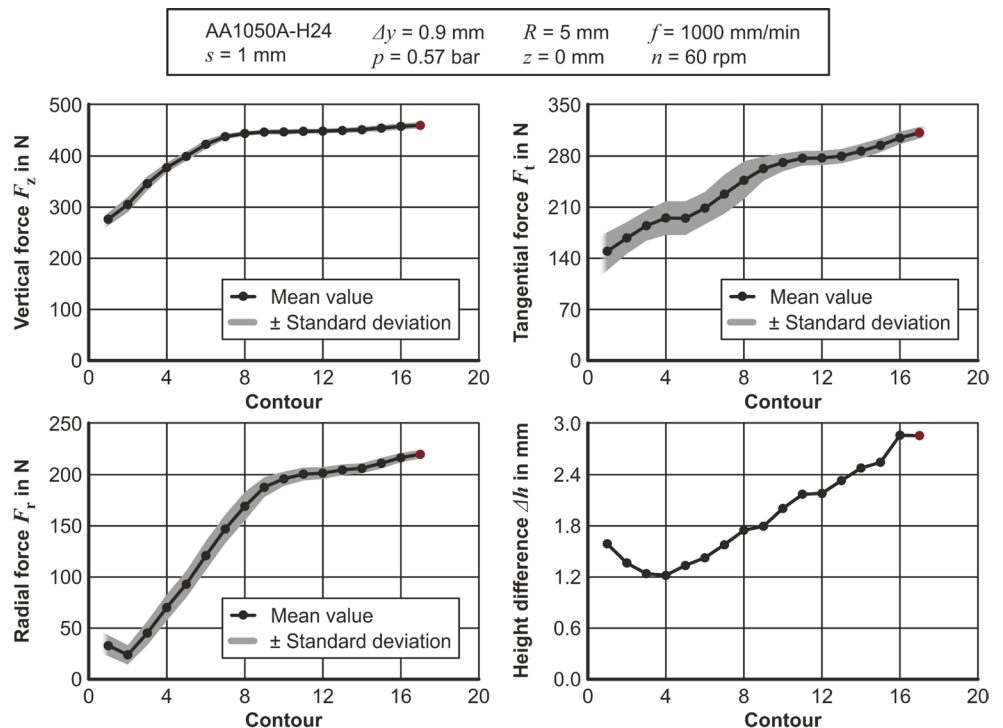
Height and force trends before failure

With the aim of understanding the mechanisms leading to failure, the trends of part height and forming forces are analyzed based on the truncated cone manufactured with a step size of $\Delta y = 0.9 \text{ mm}$ and a pressure of $p = 0.57 \text{ bar}$, Fig. 5. As the crack occurred on contour no. 18, the results are shown for the first seventeen contours of the process. The trends of the forming forces in IFAM exhibit two differences in comparison to SPIF. The force trends in SPIF are characterized by the fact that they begin at zero and increase in an initial phase after settling down in a steady-state [11]. In contrast, the pressure of the active medium permanently causes a counterforce on the tool and thus the vertical force F_z as well as the tangential force F_t start at a base level. In this regard, the radial force F_r is an exception since it starts at a low value and increases simultaneous to the emerging part wall. In addition, the force trends do not reach a steady

state under the condition of a high pressure kept constant throughout the process. The vertical force F_z and the radial force F_r both flatten after the initial phase but do not become entirely constant. The tangential force F_t gradually increases with each contour until the end of the process. Furthermore, it takes a couple of contours at the beginning until the wall of the convex geometry visibly emerges. During this period, it is possible that the height difference of each contour slightly decreases. Otherwise, the height difference will increase with each contour under a high pressure leading to an accelerated growth of the geometry. Under these conditions, both thinning and stress exceed their limit at contour no. 18, where the crack finally occurs.

The continuous measurement of the forming forces during the last complete contour and the contour with the crack are depicted in Fig. 6. Despite small fluctuations, the forces are constant throughout one contour. There are no characteristic signs such as positive or negative peaks that would indicate an imminent crack. Therefore, it is apparent that in some cases instability and cracks can occur as a spontaneous event. In this case, a sharp drop of all force components in combination with a decrease of the pressure and springback of the workpiece can be noticed. It is easy to detect cracks after they occur using any of the sensors of the set-up. However, it is the aim to predict the cracks beforehand, within the previous contours before occurrence, so that countermeasures for avoiding such an event can be taken. From the literature it is known that the occurrence of failure in SPIF is related with a decrease in the tangential force [15]. This negative trend in the tangential forming force does not exist

Fig. 5 Increasing height and force trends until failure occurs based on a spiral toolpath



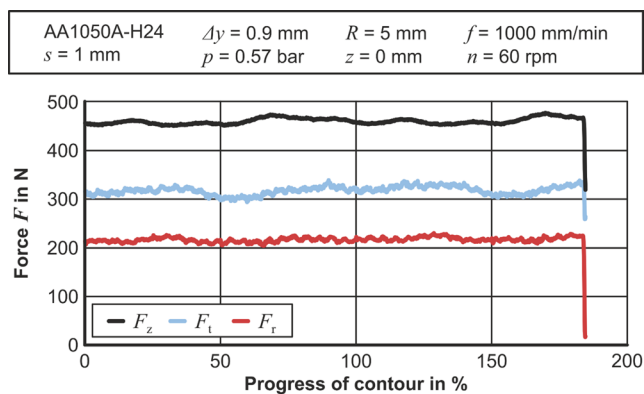


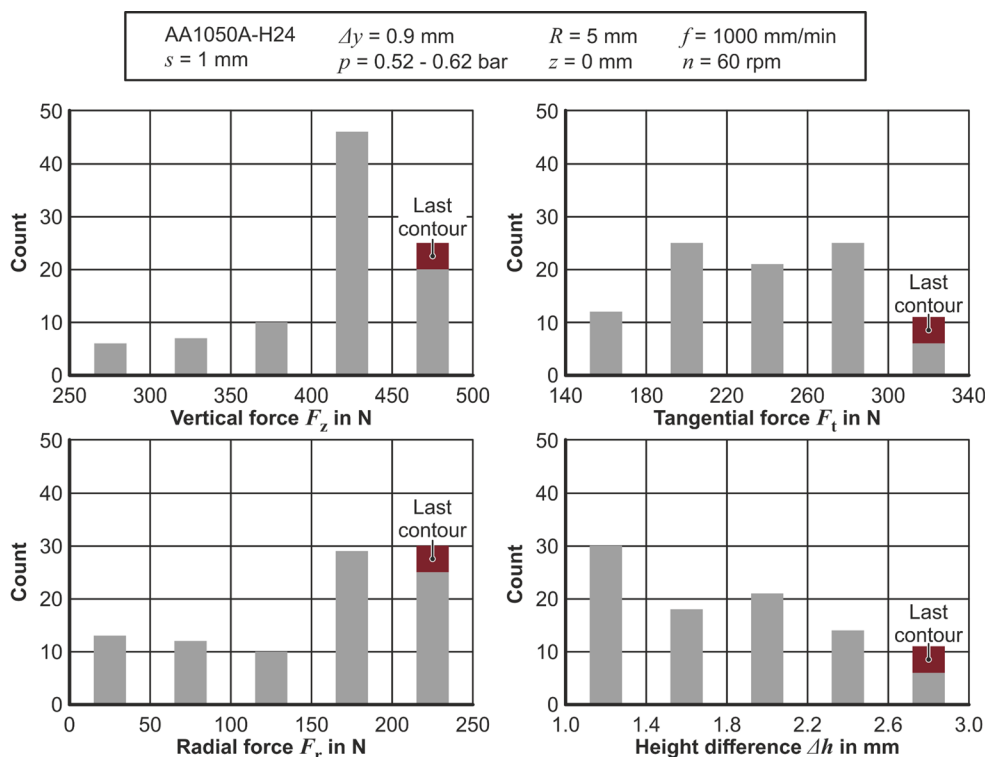
Fig. 6 Continuous force measurement in the last complete contour and in the contour in which failure occurs

prior to failure in IFAM where the behavior is characterized by increasing forming forces and an accelerating height difference. In this regard, it is necessary to identify limits of the forming force and the height difference and to analyze the correlation with failure.

Height and force limits of the forming process

The identification of the limits considering the forming forces and the height difference is discussed based on the five experiments with a step size of $\Delta y = 0.9$ mm and a pressure between $p = 0.52$ bar to 0.62 bar. The 94 contours of which five contours are the last complete contours before failure occurred are illustrated in form of a histogram, Fig. 7. In

Fig. 7 Distribution of the data for 94 contours including 5 contours before onset of cracks showing the process limits



general, situations with high values of all forming forces in addition to a high height difference will lead to cracks. The vertical force F_v and the radial force F_r have the most counts in the two upper categories and their limits are mixed with uncritical contours in the highest category. The uncritical contours show a uniform distribution regarding the tangential forming force F_t . Considering the height difference Δh , the count of uncritical contours is shifted towards the lower categories. For both the tangential forming force F_t and the height difference Δh , the number of uncritical contours in the highest category is small.

The process limits depend on several process parameters and consequently the influence of the step size Δy is addressed in accordance with the experimental plan. The final contours from all experiments ranging from $\Delta y = 0.7$ mm to 1.1 mm are summarized in Fig. 8. On the one hand, the limit of the forming forces increases with the step size Δy as could be expected since similar correlations have already been reported by Aereus et al. [12]. The tangential forming force F_t has the largest range with approx. 80 N and is also subjected to fluctuations. The vertical forming force is within a range from $F_z = 430$ N to 490 N. The range of the radial forming force F_r is the smallest of all force components, but it exhibits the smallest standard deviation. On the other hand, the range of achievable height difference Δh expands with larger step size Δy since more material can be deformed with a single contour of the toolpath. The results show that the height difference Δh has a high standard deviation for small step sizes Δy .

Fig. 8 Effect of the step size Δy on the mean values of the process limits including standard deviation

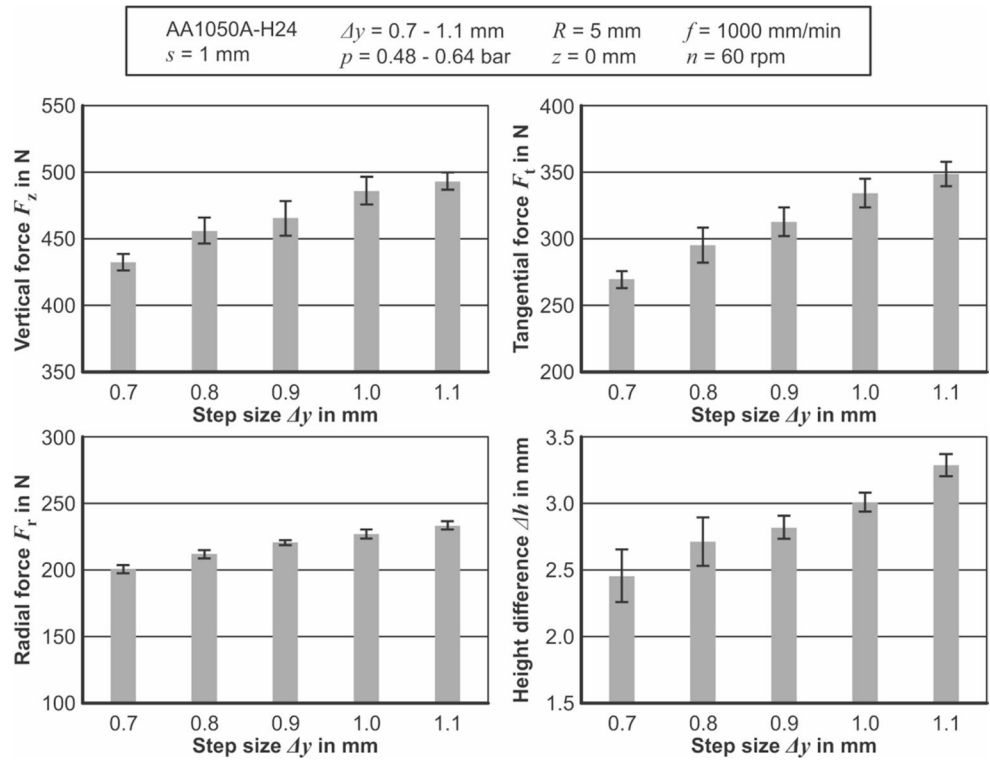
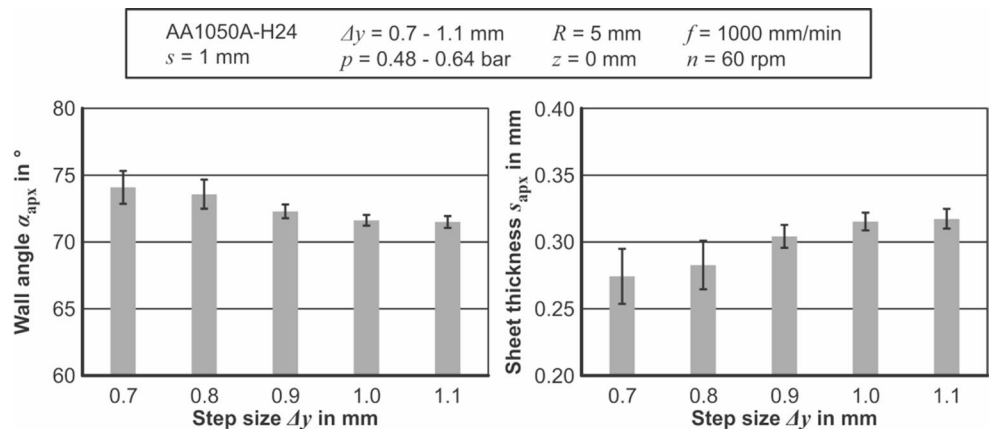


Fig. 9 Approximate values of the maximum wall angle and the minimum sheet thickness including standard deviation



The approximate values of the maximum wall angle α_{apx} and the minimum sheet thickness s_{apx} are given in Fig. 9. A wall angle above 71° and accordingly a sheet thickness under 0.33 mm must be seen as limit of the process. However, a smaller step size can slightly increase the process limit since it comes along with a lower pressure level and thus reduces stress in the forming region. Since the wall angle and the sheet thickness are in direct correlation with the height difference and the step size, the calculated variables are not included in the input data of the prediction models to avoid redundancy. Moreover, the prediction models can derive height difference and step size from the input data, which includes the part height and the tool position, due to the memory function.

Training the prediction models

Initial investigations using standard train-test splits were used to establish the architecture and explore different hyperparameter configurations. The experiments tested window lengths $\{3, 5, 7\}$, number of recurrent layers $\{1, 2, 3\}$, number of neurons per layer $\{8, 16, 64, 128\}$, learning rates $\{0.001, 0.005, 0.0001\}$ and batch sizes $\{8, 16, 32\}$. The random search conducted within this parameter space showed that the configurations including a window length of 3 contours and two recurrent layers, each containing 64 neurons, produced the most stable and optimal results, Fig. 10.

The final models in the implementation presented in the following section were trained for 250 epochs using the Adam optimizer [41], with a learning rate of 0.001 in

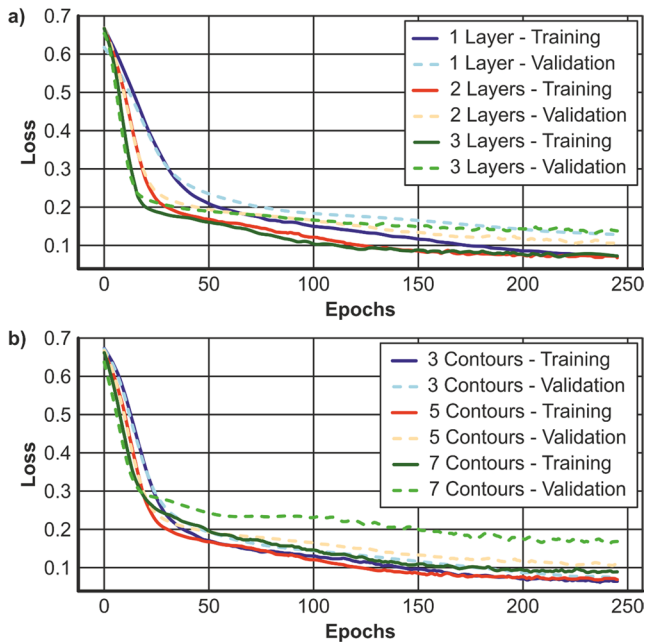


Fig. 10 Training and evaluation loss plot to compare (a) the number of recurrent layers and (b) the window lengths

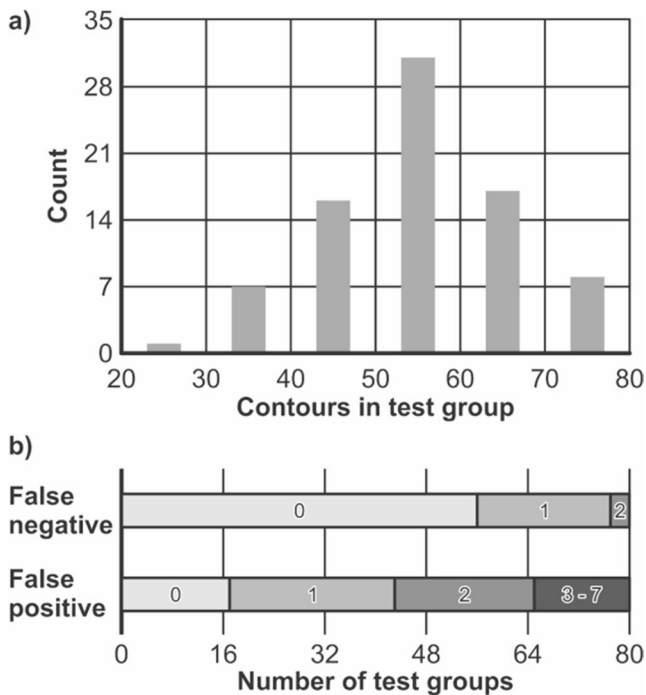


Fig. 11 Comparison of the randomly shuffled test groups in terms of (a) the distribution of test group sizes and (b) the performance measured by the count of false negative and false positive predictions

batches of 32, using a 15% dropout and a 20% recurrent dropout [42]. The hyperbolic tangent *tanh* activation function was used with a sigmoid activation function in the output layer.

Table 3 Accuracy measures of failure prediction summarized for 80 runs with a static threshold

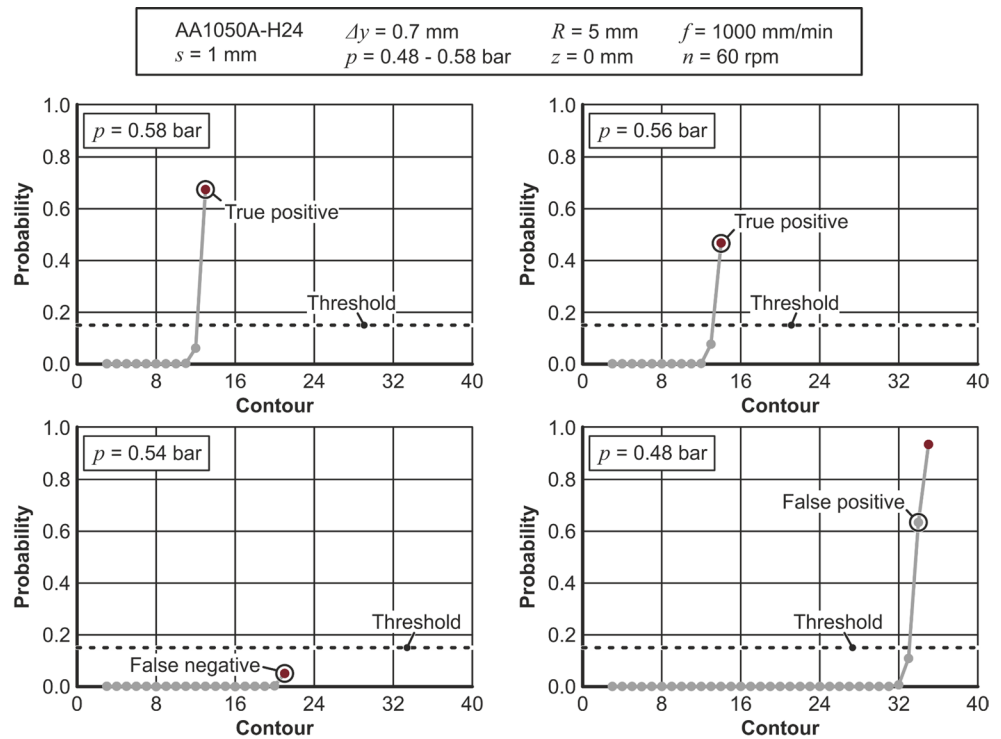
	F1 score <i>F</i>	Precision <i>P</i>	Recall <i>R</i>	Accuracy <i>A</i>
Average	0.74	0.69	0.89	0.97
Standard deviation	0.13	0.19	0.18	0.02

Evaluation of prediction accuracy

The output of the network’s sigmoid function, representing the predicted probability of failure in the next contour of manufacturing, is then compared to a defined static threshold to classify the failure prediction as either positive or negative. In the last step of this work, the prediction accuracy of the framework is evaluated and its application demonstrated for selected experiments. The performance is calculated across eighty train and validation runs and thus must be analyzed considering stochastic influences. Each test group is formed after first shuffling the experiments and consists of three experiments. Since the experiments are designed in such a way that the cracks might occur early or later in the process, the number of contours in a test group is not fixed and varies. The size distribution of the test groups is shown in Fig. 11a, indicating that most test groups contain between 50 and 60 contours, with the last three contours always being those immediately preceding failure. The threshold is optimized to achieve the maximum F1 score *F* across the inhomogeneous test groups, resulting in a value of 0.15. Based on this threshold, no false negative predictions occur in 58 test groups, indicating that in most cases, all cracks are predicted in time (Fig. 11b). In only three test groups, two out of three cracks are classified as false negatives and remain undetected. Notably, there are no test groups where the prediction entirely fails. In contrast, false positive predictions are more frequent. In the context of manufacturing processes, however, predicting failure slightly earlier is preferable to missing critical them entirely. In 26 test groups, a single false positive prediction is observed across the three experiments combined. Severe cases of false positives are rare, with only one test group exhibiting five false positives and another showing seven.

Within the data used for training and validation, most contours are uncritical, and failure predictions are expected to be negative in these cases. Since the majority of these uncritical contours are correctly classified, the overall accuracy, encompassing true negative and true positive predictions, is high. However, the performance metrics, as presented in Table 3 are affected by the limited number of critical contours within the dataset. While the F1 score *F* is maximized by adjusting the threshold, its standard deviation indicates that it is sensitive to the composition of the test groups, as is also the case for Precision *P* and the Recall *R*. Nevertheless, the metric *R* shows that approximately nine

Fig. 12 Comparison of the predicted probability of failure occurrence for accurate predictions (top), false negative predictions (bottom left) and false positive predictions (bottom right), based on the average probability across 80 runs



out of ten cracks are predicted correctly, demonstrating the potential of the method for process monitoring. Notably, this network outperforms simpler models, such as random forest ($F=0.38$) and logistic regression ($F=0.69$), particularly in its ability to generalize over unseen data.

In Fig. 12, the application of the prediction model is demonstrated on selected experiments with a horizontal step size of $\Delta y=0.7$ mm, showcasing different cases. The plots are based on the average probability across the 80 train and validation runs and begin with the third contour of the tool-path. All cases share the characteristic that the experiments start with a near-zero probability for failure occurrence and do not significantly change until towards the final contours. Shortly before the occurrence of failure, the probability sharply increases and, in cases of successful predictions, exceeds the threshold in the final contour. Nevertheless, there are two cases with a false negative or a false positive prediction. In the false negative case, the probability in the last contour fails to exceed the threshold, leading to a negative prediction. Conversely, in the false positive case, the probability for failure increases too early and overshoots the threshold before the last contour. These two cases underline the trade-off in adjusting the threshold, where reducing one type of error intensifies the other. Nonetheless, false positive predictions do not have severe consequences. As guideline for practical application, a low value should be preferred as threshold.

Applicability and transferability

The results prove the feasibility of the LSTM-based modelling approach in predicting the occurrence of failure in IFAM. The model can be integrated into the measurement and control software (Fig. 2). Its inference speed is negligible relative to the process cycle time, so that it is possible to monitor in real-time and to provide a warning when the occurrence of failure is predicted. In such cases, the pressure can be decreased manually or automatically for the following contour to avoid the failure. With decreased pressure, the forming forces and the height difference of the next contour will be reduced, ensuring that the process remains within its operational limits.

The aim was to optimize the prediction model to achieve a high F1 score for a small dataset, focusing on one geometry and one sheet material. Although the developed model performs well, its interpretability was not evaluated, thus limiting its transferability. The model provides accurate predictions for convex truncated cones that have different dimensions or that can be formed with different step sizes. However, industrial components can be made from a wide variety of materials and have complex geometries. If the process conditions change significantly, the limits of the forming forces and of the height difference will change simultaneously, making it challenging to apply the model. Once a monitoring approach is required to manufacture a specific product using IFAM, additional effort is needed for data generation and model training.

Conclusions

Pressurized air can be used in incremental sheet forming with active medium to support the bottom side of the workpiece and to create concave-convex shapes. The load applied by the active medium can cause instability of the workpiece and might lead to failure during the convex forming operation. A monitoring system capable of identifying high-risk failure situation could increase the industrial applicability of the manufacturing process. In this work, the forming behavior leading up to failure was experimentally investigated based on convex truncated cones. Consequently, a sequence-aware model employing long short-term memory was developed and tested for its applicability on the resulting experimental dataset. Its accuracy was evaluated through k -fold cross-validation with ten repetitions and different performance metrics. The following conclusions can be drawn:

- 1) In case of a high pressure being constant throughout the manufacturing process, the average forming forces during one contour and the height difference of the workpiece after each contour gradually increase. Once the process limits are reached, the likelihood of crack occurrence during subsequent contours significantly rises. The process limits depend on the amount of material deformed and are influenced by the step size.
- 2) The model consists of a sliding window, two LSTM layers and a dense layer. The length of the sliding window determines the number of consecutive contours used as input for the model. Optimal hyperparameters were identified through investigative modelling combined with a random search within a confined parameter space to minimize the loss function. The best performance was achieved using a window length of three contours, with no further improvements for window lengths of five or seven contours.
- 3) The neural network-based architecture predicts the probability of failure occurrence. Subsequently, the classification into positive and negative predictions depend on an adjustable threshold, optimized for maximizing the F1-score. Approximately nine out of ten failures can be successfully predicted by this method, proving its effectiveness. False positives are uncritical and can be accepted to some extent.

This work demonstrates that modelling approaches for sequential data, which have been successfully applied in different cases for machining according to the literature, also have potential for applications in incremental sheet forming. The accuracy of these models is heavily influenced by the amount and the structure of the data. Therefore, future

work could focus on addressing this limitation through data augmentation or transfer learning. Such approaches would enable the integration of additional process parameters such as material, sheet thickness and tool radius into the modelling framework.

Acknowledgements The authors would like to thank the German Research Foundation (DFG) for the support of the research project “manufacturing of combined convex-concave form elements by using active-medium support in incremental sheet forming” (project number: 399912095).

Author contributions Sebastian Thiery: Writing - original draft, Data curation, Methodology, Validation, Visualization. Mazhar Zein El Abdine: Writing - original draft, Data curation, Validation. Jens Heger: Writing - review & editing, Conceptualization, Supervision. Noomane Ben Khalifa: Writing - review & editing, Conceptualization, Supervision.

Funding Open Access funding enabled and organized by Projekt DEAL.

Data availability Data will be made available on request.

Declarations

Conflict of interest The authors have no relevant financial or non-financial interests to disclose.

Open Access This article is licensed under a Creative Commons Attribution 4.0 International License, which permits use, sharing, adaptation, distribution and reproduction in any medium or format, as long as you give appropriate credit to the original author(s) and the source, provide a link to the Creative Commons licence, and indicate if changes were made. The images or other third party material in this article are included in the article's Creative Commons licence, unless indicated otherwise in a credit line to the material. If material is not included in the article's Creative Commons licence and your intended use is not permitted by statutory regulation or exceeds the permitted use, you will need to obtain permission directly from the copyright holder. To view a copy of this licence, visit <http://creativecommons.org/licenses/by/4.0/>.

References

1. Emmens WC, Sebastiani G, van den Boogaard AH (2010) The technology of incremental sheet forming—a brief review of the history. *J Mater Process Technol* 210:981–997. <https://doi.org/10.1016/j.jmatprotec.2010.02.014>
2. Martins P, Bay N, Skjoedt M et al (2008) Theory of single point incremental forming. *CIRP Ann* 57:247–252. <https://doi.org/10.1016/j.cirp.2008.03.047>
3. McAnulty T, Jeswiet J, Doolan M (2017) Formability in single point incremental forming: a comparative analysis of the state of the art. *CIRP J Manuf Sci Technol* 16:43–54. <https://doi.org/10.1016/j.cirpj.2016.07.003>
4. Skjoedt M, Silva MB, Martins PAF et al (2010) Strategies and limits in multi-stage single-point incremental forming. *J Strain Anal Eng Des* 45:33–44. <https://doi.org/10.1243/03093247JSA574>

5. Vanhulst M, Lee Y, Steinfeld D (2025) ESAFORM benchmark 2024: study on the geometric accuracy of a complex shape with single point incremental forming. *Int J Mater Form*. <https://doi.org/10.1007/s12289-025-01928-1>
6. Taleb Araghi B, Manco GL, Bambach M et al (2009) Investigation into a new hybrid forming process: incremental sheet forming combined with stretch forming. *CIRP Ann* 58:225–228. <https://doi.org/10.1016/j.cirp.2009.03.101>
7. Meier H, Magnus C, Smukala V (2011) Impact of superimposed pressure on dieless incremental sheet metal forming with two moving tools. *CIRP Ann* 60:327–330. <https://doi.org/10.1016/j.cirp.2011.03.134>
8. Ben Khalifa N, Thiery S (2019) Incremental sheet forming with active medium. *CIRP Ann* 68:313–316. <https://doi.org/10.1016/j.cirp.2019.04.043>
9. Thiery S, Zein El Abdine M, Heger J (2021) Closed-loop control of product geometry by using an artificial neural network in incremental sheet forming with active medium. *Int J Mater Form* 14:1319–1335. <https://doi.org/10.1007/s12289-020-01598-1>
10. Duflo JR, Habraken A-M, Cao J et al (2018) Single point incremental forming: state-of-the-art and prospects. *Int J Mater Form* 11:743–773. <https://doi.org/10.1007/s12289-017-1387-y>
11. Duflo JR, Tunçkol Y, Szekeres A et al (2007) Experimental study on force measurements for single point incremental forming. *J Mater Process Technol* 189:65–72. <https://doi.org/10.1016/j.jmatprotec.2007.01.005>
12. Aerens R, Eyckens P, van Bael A et al (2010) Force prediction for single point incremental forming deduced from experimental and FEM observations. *Int J Adv Manuf Technol* 46:969–982. <https://doi.org/10.1007/s00170-009-2160-2>
13. Petek A, Kuzman K, Suhač B (2009) Autonomous on-line system for fracture identification at incremental sheet forming. *CIRP Ann* 58:283–286. <https://doi.org/10.1016/j.cirp.2009.03.092>
14. Ambrogio G, Filice L, Micari F (2006) A force measuring based strategy for failure prevention in incremental forming. *J Mater Process Technol* 177:413–416. <https://doi.org/10.1016/j.jmatprotec.2006.04.076>
15. Filice L, Ambrogio G, Micari F (2006) On-line control of single point incremental forming operations through punch force monitoring. *CIRP Ann* 55:245–248. [https://doi.org/10.1016/S0007-8506\(07\)60408-9](https://doi.org/10.1016/S0007-8506(07)60408-9)
16. Fiorentino A (2013) Force-based failure criterion in incremental sheet forming. *Int J Adv Manuf Technol* 68:557–563. <https://doi.org/10.1007/s00170-013-4777-4>
17. Gao RX, Krüger J, Merklein M et al (2024) Artificial intelligence in manufacturing: state of the art, perspectives, and future directions. *CIRP Ann* 73:723–749. <https://doi.org/10.1016/j.cirp.2024.04.101>
18. Cao J, Bambach M, Merklein M et al (2024) Artificial intelligence in metal forming. *CIRP Ann* 73:561–587. <https://doi.org/10.1016/j.cirp.2024.04.102>
19. Nagargoje A, Kankar PK, Jain PK (2023) Application of artificial intelligence techniques in incremental forming: a state-of-the-art review. *J Intell Manuf* 34:985–1002. <https://doi.org/10.1007/s10845-021-01868-y>
20. Ambrogio G, Filice L (2009) Application of neural network technique to predict the formability in incremental forming process. *KEM* 410:381–389. <https://doi.org/10.4028/www.scientific.net/KEM.410-411.381>
21. Ambrogio G, Filice L, Guerriero F (2011) Prediction of incremental sheet forming process performance by using a neural network approach. *Int J Adv Manuf Technol* 54:921–930. <https://doi.org/10.1007/s00170-010-3011-x>
22. Liu Z, Li Y (2020) Small data-driven modeling of forming force in single point incremental forming using neural networks. *Eng Comput* 36:1589–1597. <https://doi.org/10.1007/s00366-019-00781-6>
23. Duan S, Kozjek D, Mehr E (2024) Forming force prediction in double-sided incremental forming via GNN-based transfer learning. *J Manuf Process* 120:867–877. <https://doi.org/10.1016/j.jmapro.2024.04.093>
24. Pimenov DY, Bustillo A, Wojciechowski S et al (2023) Artificial intelligence systems for tool condition monitoring in machining: analysis and critical review. *J Intell Manuf* 34:2079–2121. <https://doi.org/10.1007/s10845-022-01923-2>
25. Farahani MA, McCormick MR, Gianinny R et al (2023) Time-series pattern recognition in smart manufacturing systems: a literature review and ontology. *J Manuf Syst* 69:208–241. <https://doi.org/10.1016/j.jmsys.2023.05.025>
26. Manjunath K, Tewary S, Khatri N (2022) Surface roughness prediction in milling using long-short term memory modelling. *Mater Today Proc* 64:1300–1304. <https://doi.org/10.1016/j.matpr.2022.04.126>
27. Ma J, Luo D, Liao X et al (2021) Tool wear mechanism and prediction in milling TC18 titanium alloy using deep learning. *Measurement* 173:108554. <https://doi.org/10.1016/j.measurement.2020.108554>
28. Peng D, Li H, Dai Y et al (2022) Prediction of milling force based on spindle current signal by neural networks. *Measurement* 205:112153. <https://doi.org/10.1016/j.measurement.2022.112153>
29. Chen Z, Liu Y, Valera-Medina A et al (2021) Multi-faceted modelling for strip breakage in cold rolling using machine learning. *Int J Prod Res* 59:6347–6360. <https://doi.org/10.1080/00207543.2020.1812753>
30. Meyes R, Donauer J, Schmeing A et al (2019) A recurrent neural network architecture for failure prediction in deep drawing sensory time series data. *Procedia Manuf* 34:789–797. <https://doi.org/10.1016/j.promfg.2019.06.205>
31. Jeswiet J, Micari F, Hirt G et al (2005) Asymmetric single point incremental forming of sheet metal. *CIRP Ann* 54:88–114. [https://doi.org/10.1016/S0007-8506\(07\)60021-3](https://doi.org/10.1016/S0007-8506(07)60021-3)
32. Thiery S, Zein El Abdine M, Heger J et al (2025) Manufacturing of irregular shapes through force control in incremental sheet forming with active medium. *Adv Ind Manuf Eng* 10:100157. <https://doi.org/10.1016/j.aime.2025.100157>
33. Jeswiet J, Young D (2005) Forming limit diagrams for single-point incremental forming of aluminium sheet. *Proceedings of the Institution of Mechanical Engineers, Part B: Journal of Engineering Manufacture* 219:359–364. <https://doi.org/10.1243/095440505X32210>
34. Chen G (2016) A gentle tutorial of recurrent neural network with error backpropagation. <http://arxiv.org/pdf/1610.02583v3>
35. Hochreiter S, Schmidhuber J (1997) Long Short-term memory. *Neural Comput* 9:1735–1780
36. Cho K, van Merriënboer B, Bahdanau D et al (2014) On the Properties of Neural Machine Translation: Encoder-Decoder Approaches. <http://arxiv.org/pdf/1409.1259v2>
37. Chung J, Gulcehre C, Cho K et al (2014) Empirical Evaluation of Gated Recurrent Neural Networks on Sequence Modeling. <http://arxiv.org/pdf/1412.3555v1>
38. Studer S, Bui TB, Drescher C et al (2021) Towards CRISP-ML(Q): a machine learning process model with quality assurance methodology. *MAKE* 3(2):392–413. <https://doi.org/10.3390/make3020020>
39. Schröer C, Kruse F, Gómez JM (2021) A systematic literature review on applying CRISP-DM process model. *Procedia Comput Sci* 181:526–534. <https://doi.org/10.1016/j.procs.2021.01.199>
40. Sitaula C, Shahi TB (2022) Monkeypox virus detection using pre-trained deep learning-based approaches. *J Med Syst* 46:78. <https://doi.org/10.1007/s10916-022-01868-2>

41. Kingma DP, Ba J (2014) Adam: A Method for Stochastic Optimization. <http://arxiv.org/pdf/1412.6980v9>
42. Semeniuta S, Severyn A, Barth E (2016) Recurrent Dropout without Memory Loss. <http://arxiv.org/pdf/1603.05118v2>

Publisher's note Springer Nature remains neutral with regard to jurisdictional claims in published maps and institutional affiliations.